International Journal of Impact Engineering, Volume 107, September 2017, Pages 1–11
DOI: 10.1016/j.ijimpeng.2017.05.003

Strain rate dependence of mode II delamination resistance in through thickness reinforced laminated composites

Mehdi Yasaee[a*], Galal Mohamed[b], Antonio Pellegrino[c], Nik Petrinic[c], Stephen R. Hallett[b]

*a School of Aerospace, Transport and Manufacturing, Building 83, University of Cranfield, Cranfield, MK43 0AL, UK *m.yasaee@cranfield.ac.uk*

b Advanced Composites Centre for Innovation and Science (ACCIS), University of Bristol, Queen's Building, University Walk, Bristol, BS8 1TR, UK

c Department of Engineering Science, Engineering and Technology Building, Parks Road, Oxford OX1 3PJ

Abstract

A thorough experimental procedure is presented in which the mode II delamination resistance of a laminated fibre reinforced plastic (FRP) composite with and without Z-pins is characterised when subjected to increasing strain rates. Standard three-point End Notched Flexure (3ENF) specimens were subjected to increasing displacement loading rates from quasi-static (~0m/s) to high velocity impact (5m/s) using a range of test equipment including drop weight impact tower and a Modified Hopkinson Bar apparatus for dynamic three-point bending tests.

The procedure outlined uses compliance based approach to calculate the fracture toughness which was shown to produce acceptable values of G_{IIC} for all loading rates. Using detailed high resolution imaging relationships between delamination velocities, apparent fracture toughness, longitudinal and shear strain rates were measured and compared. Confirming behaviours observed in literature, the thermosetting brittle epoxy composite showed minor increase in G_{IIC} with increase in strain rate. However, the Z-pinned specimens showed a significant increase in the apparent G_{IIC} with loading rate. This highlights the need to consider the strain rate dependency of the Z-pinned laminates when designing Z-pinned structures undergoing impact.

Keywords

Composites; delamination; impact; fracture toughness; Z-pin

Published by Elsevier. This is the Author Accepted Manuscript issued with:
Creative Commons Attribution Non-Commercial No Derivatives License (CC:BY:NC:ND 4.0).
The final published version is available online at 10.1016/j.ijimpeng.2017.05.003 .
Please refer to any applicable publisher terms of use.

1 Introduction

Environmental, financial and performance requirements in global transport and energy industries necessitates ever more fuel efficient and high performance engineering structures and components. One method to tackle all of these requirements is to reduce the weight of components whilst maintain the same structural performance. For this reason laminated composite materials have seen an increased usage across all these sectors. These materials provide exceptional specific stiffness relative to their metal counter parts, amongst many other benefits such as corrosive resistance and fatigue performance.

However, the use of laminated composites does possess some drawbacks. The anisotropy of the material and manufacturing challenges results in a costly product development cycle. Furthermore, laminated composites do not possess any through thickness reinforcements, hence a major failure mechanisms of these materials is de-bonding or delamination of individual ply layers. Although, composite components are by design, capable of carrying in-service stresses, localised out of plane loading in form of impact may generate delamination damage, which will significantly reduce the residual strength of the component.

To overcome this limitation it is possible to adopt many ‘damage tolerant design’ techniques. Thicker and thus stiffer components will make them more resilient to out of plane loading but with a weight penalty. Use of tougher matrix constituents with a plastic phase will improve the overall performance but only up to a limit [1,2]. Use of interleaving materials at the critical interfaces where delaminations may initiate is another popular method [3,4]. Modern composite systems are increasingly employing such technologies, which have provided significant performance enhancements compared to earlier generations of composite materials.

For largescale delamination damage, through thickness reinforcement (TTR) technologies have been shown to be quite effective [5]. In these methods, fibres or small rods are inserted in the composite materials reinforcing the thickness direction of the laminate. One of these techniques, also known as Z-pinning is a popular method used to reinforce pre-preg composite laminates. By inserting small stiff, fibrous composite rods in the thickness direction, this helps bridge the delamination interface tractions and thus provides excellent damage resistance capability [6].

Resistance of TTR composites to delamination has been subject to many studies, including quasi-static [6–8] and fatigue loading [9]. However, experimental investigations on the response of TTR composites when subjected to dynamic loading is limited and not well understood.

Investigations on the strain rate dependency of the constitutive mechanical properties of composite materials has produced many contradicting results as highlighted by Gerlach *et. al.* [10]. Investigations have shown tensile strength and stiffness can either increase, decrease or be independent of strain rate. Strain rate dependency of delamination fracture toughness has also exposed conflicting results as reviewed comprehensively by Jacob *et. al.* [11], highlighting experimental investigations that have demonstrated increases, decreases and independence of fracture toughness with strain rates. However from a closer look at the literature, some trends becomes apparent. For thermosetting un-toughened epoxy composites, delamination fracture toughness has either an increase [12–14] or no significance [15,16] with increased loading rate. Whereas thermoplastic composites have shown strong negative strain rate dependency, with delamination fracture toughness decreasing with increase in loading rate [15,17–19]. Ductile thermoplastics materials are well known to exhibit

brittle fracture when subjected to increased strain rates [20], whereas fracture in brittle epoxies do not exhibit as strong strain rate dependence [21].

Dynamic fracture of materials is a specialist field of interest in material engineering [22] with a wide range of studies exploring fracture of materials from the fundamental atomic scale to large geological cases. Of particular interest is the concept of a limiting speed of crack propagation rate ($\dot{a} = \partial a/\partial t$) which has been shown to be equal to the materials' shear wave speed (C_s) when loaded in mode I, whilst in mode II the delamination rate can increase beyond the shear wave speed reaching a critical velocity (V_C) which is approximately equal to $\sqrt{2}C_S$ [23]. These extreme shear crack velocities have been achieved in edge notched composite plates where loading is directly transferred to the generation of the crack front, through a specific 1point bend configuration. Measuring crack velocities is challenging and often requires special detection gauges [24] or high resolution, high speed photography in excess of 50,000 frames per second (fps) to deduce the crack tip propagation reliably. For this reason only a few investigations exist in literature where delamination velocity in a standard fracture test has been measured. In mode I using a double cantilever beam (DCB), delamination speeds have been shown to reach up to 20-80m/s [15] for loading rate of 10m/s. In mode II delamination speeds have shown to reach up to 130m/s using an end loaded split (ELS) specimen [25]. Tsai *et. al.* [24] and Guo et. al. [26] used a specific quasi-static test setup in which strain energy at the crack tip was built up with the use of interleaved toughening strips in a 3ENF and DCB specimen respectively. This build of strain energy in the sample thus allowed for control of the propagation rate of the delamination. Using this technique delamination speeds of up to 1100m/s in mode II and 330m/s in mode I were reported, respectively.

It is quite evident that loading rate will only influence the fracture toughness of a material when the stress waves travelling in the body directly alter the stress states in the plastic zone ahead of a crack tip. For this reason factors such as loading/boundary conditions as well as geometric shape of the component will greatly influence the dynamic response of a component. Therefore direct comparison of the loading, strain and crack propagation cannot be readily made and could be one major reasons behind contradicting results in literature, particularly in regard to epoxy based composite delaminations.

A feature unique to laminated composites that has shown to have a direct dependence on strain rate is the apparent mode II fracture toughness of interlaminar toughening techniques such as interleaving or TTR. Jiang et. al. [27] showed a direct linear increase in fracture toughness of a thermosetting composite with a toughened epoxy interleave phase. With a modest loading rate increase of 1-100mm/min up to 84% increase in apparent G_{IIC} was reported. Colin de Verdiere et. al. [25] reported a modest increase of approximately 26% in the initiation apparent G_{IIC} of tufted composite specimens loaded up to a rate 7m/s. For Z-pinned composites the mode I apparent fracture toughness appears to reduce with an increase in loading rate as shown by Liu et. al. [28].

There are very few papers in the open literature concerned with the strain rate dependency of Z-pinned composites (e.g. [29]). The objective of this paper was to investigate the mode II aparent fracture toughness of a laminated composite reinforced in the thickness direction using with Z-pins made from carbon fibre reinforced plastic (CFRP) rods. These tests were carried out at displacement loading rates from quasi-static up to 5m/s. A comprehensive analysis of the composite

response was made to conclusively show the effect of strain rate on the delamination resistance in un-reinforced and TTR epoxy based composites.

2 Experimental test procedure

2.1 Materials and specimen preparation

Specimens were manufactured using IM7/8552 prepreg (Hexcel, UK) stacked in a Zero Dominated (ZD) sequence of $[(0,-45,0,+45)_{3S}]_S$ to achieve a nominal thickness of 6mm, with a 13μm PTFE film placed at the mid plane interface to form a starter crack, which falls between two 0° plies, preventing any out of plane crack migration. The effective laminate properties were calculated using laminate theory and anisotropic material properties of a single UD ply (Table 1) with axis definitions as shown in Figure 2. The test procedure followed the standard 3 point bend end notched flexure (3ENF) [30] shown in Figure 1 with varying loading displacement rates ($\dot{\delta}$).

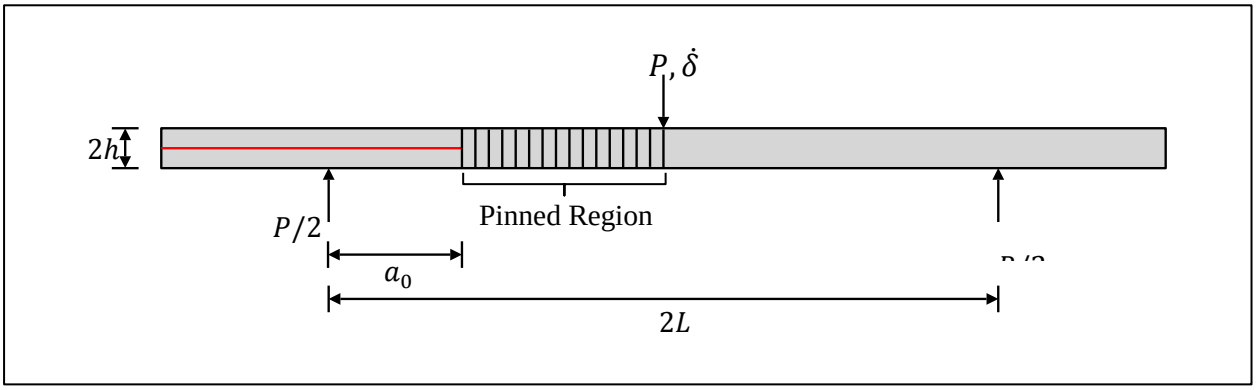

Figure 1 3ENF test setup

The Z-pinned specimens where pinned with T300 carbon/BMI pins arranged in a grid pattern with a spacing of 1.75mm, generating a nominal 2% areal density. Both the control and the Z-pinned samples were machined from a single plate, ensuring consistency in the material properties across both sample sets.

Table 1 Effective Properties IM7/8552 laminate in a (0, -45, 0, +45) stacking sequence

$\mathbf{E_1}$	90.83GPa	$\mathbf{G_{12}}$	23.37GPa	$\mathbf{\nu_{12}}$	0.71
$\mathbf{E_2}$	26.44GPa	$\mathbf{G_{13}}$	4.86GPa	$\mathbf{\nu_{13}}$	0.14
$\mathbf{E_3}$	13.18GPa	$\mathbf{G_{23}}$	4.23GPa	$\mathbf{\nu_{23}}$	0.37

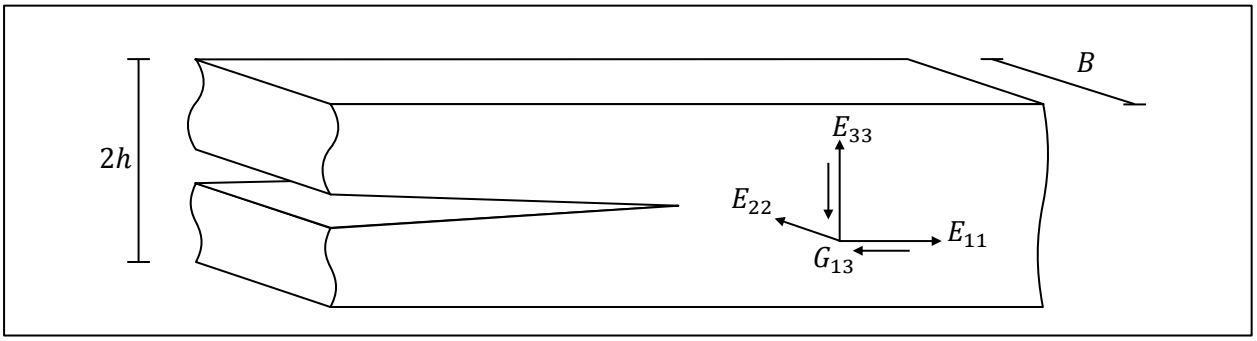

Figure 2 Composite laminate axis definitions

2.2 Specimen Preparation

Each specimen was machined to a nominal width of 20mm. The un-cracked part of each individual specimen was tested in a 3 point bend (3PB) following the ASTM-790 [31] test standard to measure the flexural modulus (E_{1f}) of the material. The width (B) and thickness ($2h$) of each specimen was measured at three different locations along its length to an accuracy of ±0.05mm. For each specimen, a natural mode II pre-crack from the starter film was created using the procedure set out in ASTM-D7905 [30] to generate an initial crack length (a_0) of 20mm when positioned in the final test configuration. This resulted in 30mm of uncracked laminate and reinforced region ahead of the crack for the control and Z-pinned samples respectively. To ensure that the initial crack length was correctly determined, each sample was non-destructively tested using an ultrasonic C-scan technique and the average crack front measured as shown in Figure 3.

Each edge of the specimens was painted with a speckle pattern to measure full field strain and obtain accurate displacement measurements.

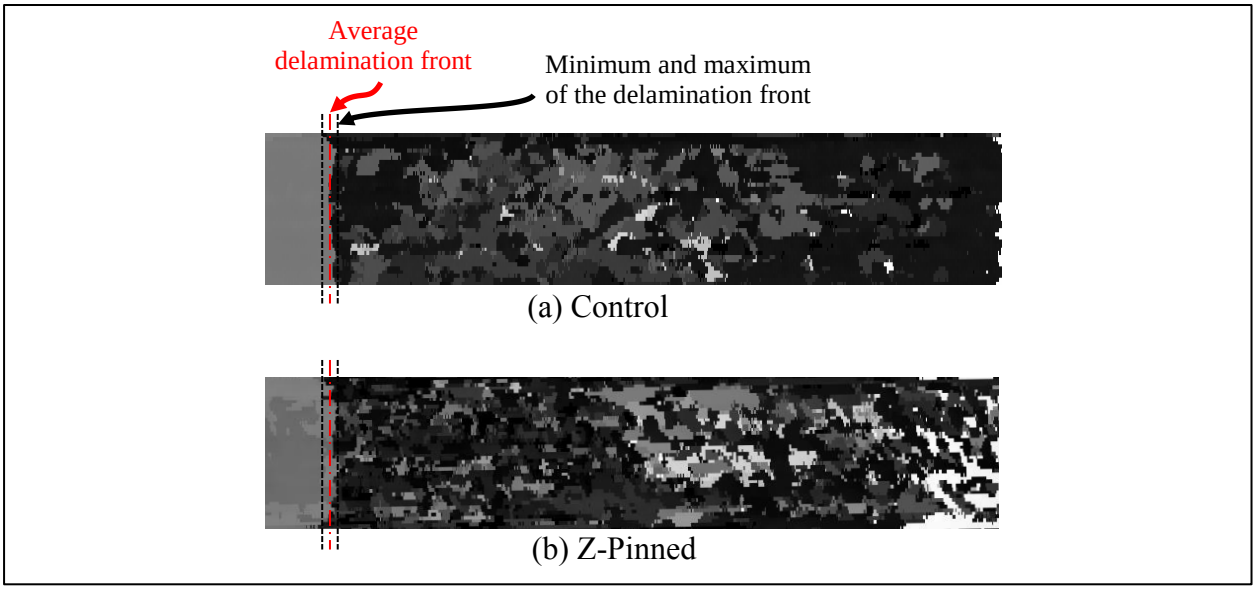

Figure 3 Example of ultrasonic C-scan of (a) control and (b) pinned samples to determine the average natural pre-crack position

2.3 Test procedures

The ENF tests were performed with increasing displacement loading rates from quasi-static (8.3×10^{-6}m/s), to intermediate (1-4m/s) and high (5.5m/s) on three different test apparatus. For all tests the support roller half span (L) was set at 50mm with an initial crack length (a_0) of 20mm and support roller and loading nose diameter of 10mm. The displacement and the crack propagation for all tests was monitored using a high definition imaging for quasi-static tests and high speed photography with a minimum of 100,000fps for the high loading rate tests. The camera was set up to ensure on average a 12pixel to mm resolution. This ensured sufficient resolution was available for full field strain measurements.

2.4 Quasi-static

The quasi-static 3ENF tests were carried out according to the ASTM-D7905 [30] standard with a loading displacement rates of 0.5mm/min (8.3×10^{-6}m/s). The load was

measured using a calibrated 5kN load cell on a hydraulic Instron test machine. For these tests, the delamination is unstable for the length of the specimen being measured. Therefore, the maximum load corresponds to the initiation of delamination which is the critical load to use in the data reduction equations.

2.5 Intermediate tests

Intermediate loading displacement rate 3ENF tests were carried out on an instrumented drop weight impact tower. For these tests a cylindrical loading nose was attached to the end of a calibrated piezo-electric load-cell. The loading displacement rate was varied by raising the entire impactor unit weighing 6.21 kg to a specific height above the top surface of the laminate.

2.6 High rate tests

High loading displacement rate 3ENF tests were carried out using a Modified Hopkinson Bar apparatus shown in Figure 4. The setup follows closely the impact bending test procedure carried out by Hallett [32], Gerlach et. al. [33] and Wiegand et. al. [34]. A striker bar of length L_{str}, is accelerated using compressed air to strike an instrumented impactor bar of length L_{imp} with the same mechanical impedance and diameter. This impact then generates a stress pulse of duration of $2L_{str}/c_0$, where $c_0 = \sqrt{E/\rho}$ is the 1D longitudinal wave speed in the bar termed bar velocity. It is desirable to position the first strain gauge at a distance of $d_1$such that $L_{str} < (L_{imp} - d_1)$ to ensure that the incident pulse and the first reflected pulse from the striker bar does not superimpose. This transfer of kinetic energy then accelerates the impactor bar to a specific impact velocity generating the loading rate required to deform the specimen. The material and geometrical properties for both the striker and the impact bar and the strain gauge positions are given in Table 2.

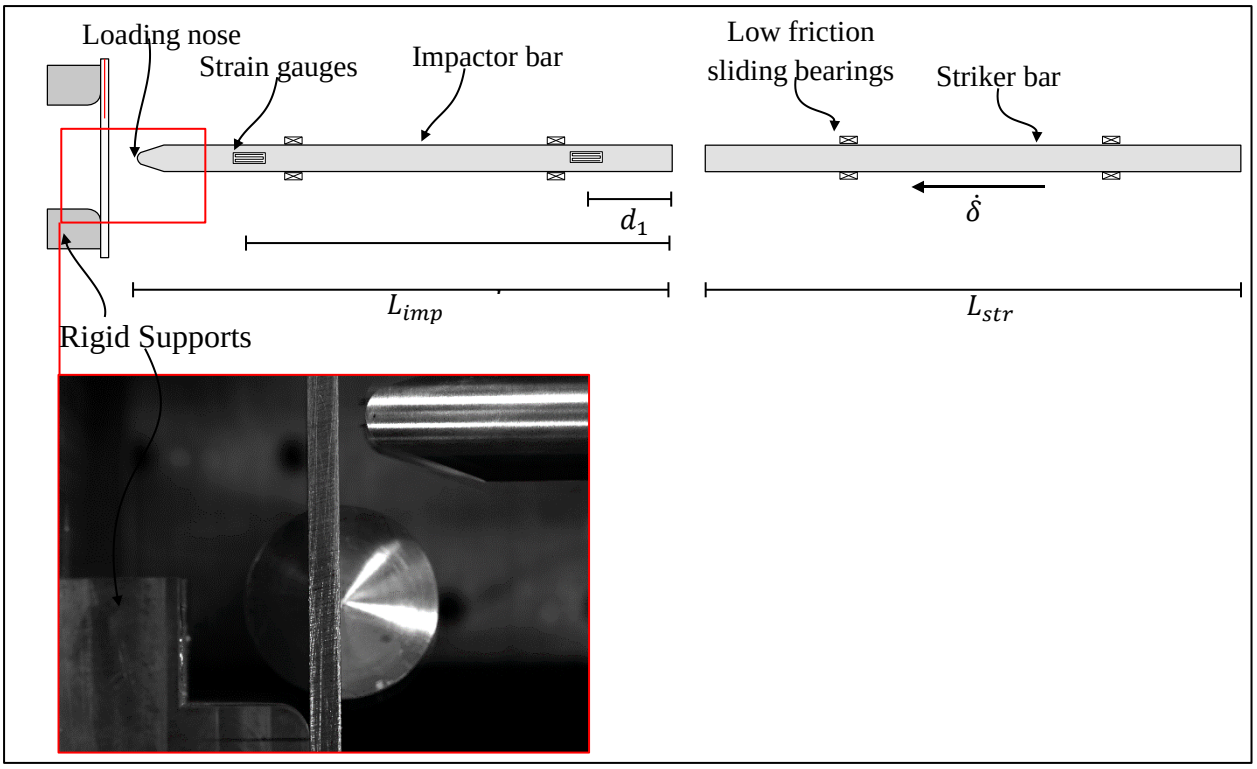

Figure 4 SHPB test setup

Table 2 SHPB Properties

Material	Titanium Alloy Ti-6Al-4V (Grade 5)
Modulus, *E*	113.8GPa
Density, ρ	4430kg/m^3
Striker Bar	
Length, L_{str}	2.7m
Diameter	20mm
Mass	3.758kg
Impactor Bar	
Length, L_{imp}	3.0m

Diameter	20mm
Mass	4.175kg
Strain gauge 1, d_1	0.215m
Strain gauge 2, d_2	1.806m

208

209 Using two strain gauge stations set up in a half-bridge configuration on the impact bar
210 the magnitude of the stresses at those specific cross section in the bar can be
211 calculated. The motion of longitudinal waves in a cylindrical bar can be described
212 using the one-dimensional wave equation:

$$\frac{\partial^2 u}{\partial x^2} = \frac{1}{c_0^2}\frac{\partial^2 u}{\partial t^2} \tag{1}$$

213 The general solution to this wave equation can be expressed in terms of two arbitrary
214 functions, f and g that define the wave-forms traveling in the positive (forwards) and
215 negative (backwards) directions respectively.

$$u(x,t) = f(x - c_0 t) + g(x + c_0 t) \tag{2}$$

216 Following standard constitutive relationships, this can be written in the form:

$$\frac{du(x,t)}{dx} = \varepsilon(x,t) = f'(x - c_0 t) + g'(x + c_0 t) = \varepsilon_1(x,t) + \varepsilon_2(x,t) \tag{3}$$

217 Where, $f'(x - c_0 t)$ and $g'(x + c_0 t)$ are replaced by the incident and reflected
218 strain functions $\varepsilon_1(x,t)$ and $\varepsilon_2(x,t)$ respectively. The stress σ and particle velocity
219 v at any point in the bar can also be defined using equation (3) as:

$$\sigma(x,t) = E\big(\varepsilon_1(x,t) + \varepsilon_2(x,t)\big) \tag{4}$$

$$v(x,t) = -\frac{E}{\rho c_0}\big(\varepsilon_1(x,t) - \varepsilon_2(x,t)\big) \tag{5}$$

220 Where ρ is the density, E is the modulus and c_0 is the 1D impactor bar velocity.

221 Figure 5 shows the Langrangian (time-distance) diagram for a 1D wave propagation

222 in a cylindrical bar of length L_{imp} with two strain gauges at a distance d_1 and d_2 from

223 the striker/impactor contact end ($x = 0$). It is possible to calculate the total stress in

224 any cross section of the bar including the tip of the impactor using the time shifted

225 values from the strain gauge instrumentations. In this investigation the location of

226 interest was at the impactor tip, $x = L_{imp}$. The forward and backward travelling

227 elastic strain waves at this location was determined using the following routine:

$$\varepsilon_1\big(L_{imp}, t\big) = \begin{cases} \varepsilon[d_1, t - (t_3 - t_1)] & t < t_4 \\ \varepsilon[d_1, t - (t_3 - t_1)] - \varepsilon_2\big[L_{imp}, t - (t_4 - t_1)\big] & t \geq t_4 \end{cases} \tag{6}$$

$$\varepsilon_2(L, t) = \begin{cases} \varepsilon[d_2, t + (t_3 - t_2)] - \varepsilon[d_1, t + (t_3 - t_2) - (t_2 - t_1)] & t < t_4 \\ \varepsilon[d_2, t + (t_3 - t_2)] - \big\{\varepsilon[d_1, t + (t_3 - t_2) - (t_2 - t_1)] - \varepsilon_2\big[L_{imp}, t - 2(t_2 - t_1)\big]\big\} & t \geq t_4 \end{cases} \tag{7}$$

228 Using equations (6), (7) and (4) the load at the end of an impactor bar with a cross

229 section area, A is:

$$F\big(L_{imp}, t\big) = A\sigma\big(L_{imp}, t\big) \tag{8}$$

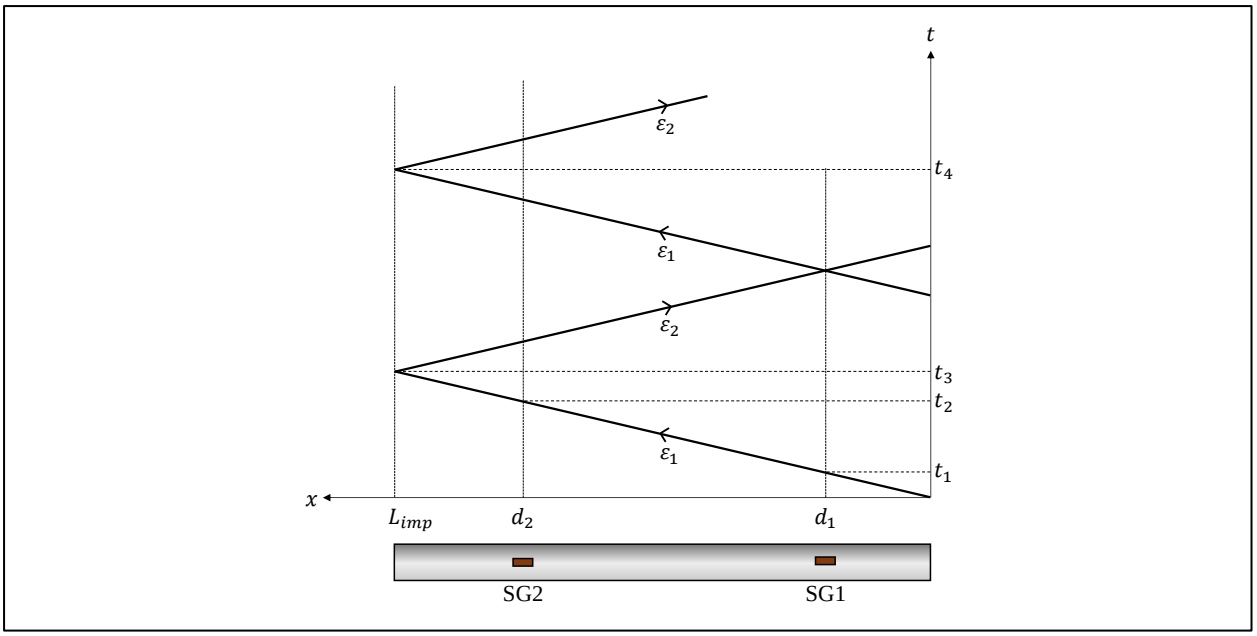

Figure 5 Langrangian diagram for longitudinal waves in cylindrical bar

The load signal calculated was further filtered to remove high frequency noise. A 1000th order 1D median filter was found to effectively attenuate the high peak signals which was not possible with a 500 point moving average smoothing technique, Figure 6. This plot also illustrates the load drops associated with delamination initiation and subsequent fracture, as confirmed by the high speed footage.

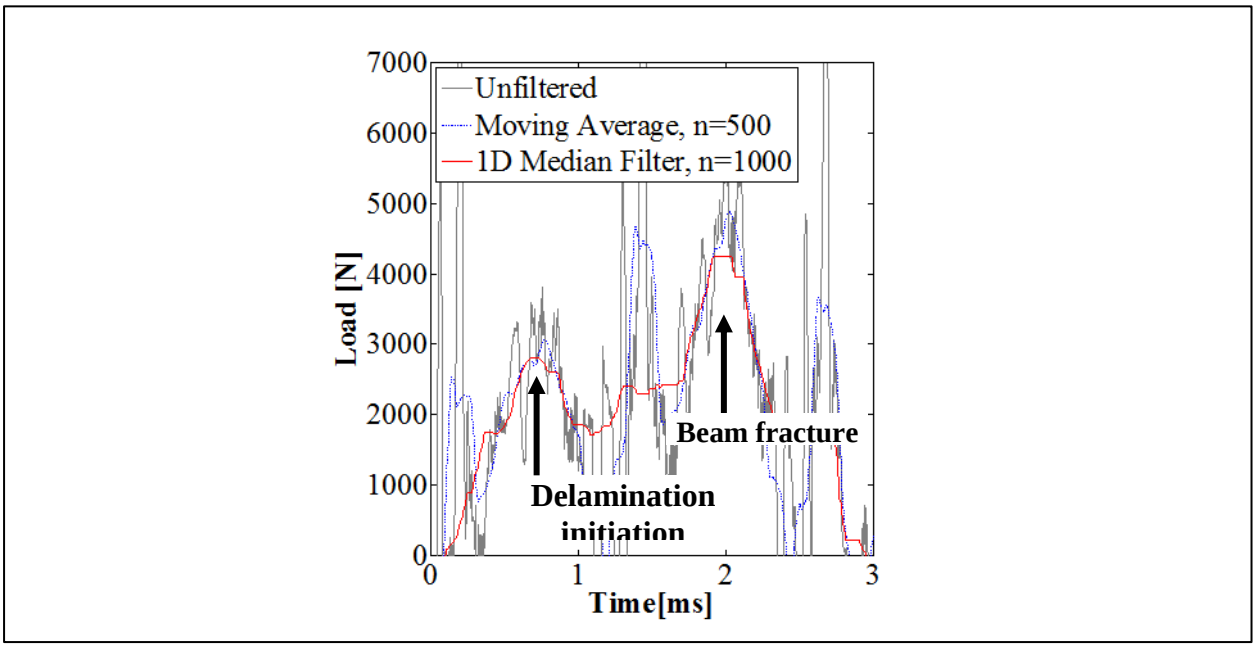

Figure 6 Example of filtration of the calculated load from the SHPB tests

The wedge shaped tip of the impactor was designed in order to minimise the effect of stress wave reflections along the impactor rod tip. Gerlach et. al. [33] and Wiegand et. al. [34] have shown using FE analysis that the force obtained from stress wave analysis compares well to the numerical simulations confirming that any inaccuracy introduced by the geometry of the wedged tip is negligible.

2.7 Data reduction technique

Load response of a high rate test procedures suffer from high frequency oscillations arising from dynamic effects as shown in previous section. The load output from the drop-weight impact tower used in these experiments is filtered internally by the test equipment which removes high frequency vibrations however inertial oscillations are still visible in the response. These dynamic effects also increase with increasing loading rates, thereby determining the critical load at the moment of initiation is not possible [15]. For this reason, use of measured critical load in the data reduction calculations will yield incorrect values of the materials fracture toughness.

It has been shown that CFRP laminates exhibit no observable strain rate dependency in their axial modulus E_{11} [15,35]. It is thus possible to calculate G_{IIC} using the displacement at the moment of delamination initiation. This displacement can be reliably measured using the high speed photography images from all loading rate test procedures. The compliance of the 3ENF specimen [36] is given by:

$$C = \frac{2L^3 + 3a^3}{8E_{1f}Bh^3} + \frac{3L}{10G_{13}Bh} \tag{9}$$

The term on the right includes the influence of through thickness shear which is dependent on the h/L of the test setup. The inter-laminar fracture toughness is calculated by measuring the strain energy release rate of the material, defined as:

$$G = \frac{1}{B}\frac{\partial(W-U)}{\partial a} \tag{10}$$

where W is the work applied by external forces and U is the elastic strain energy.

Using equation (10) the mode II fracture toughness has been reduced [37] to be:

$$G_{IIC} = \frac{9\left(\frac{\delta}{C}\right)^2 (a+0.42\chi h)^2}{16B^2 E_{1f} h^3} \tag{11}$$

$$\chi = \left[\frac{E_{11}}{11G_{13}}\left(3-2\left(\frac{\Gamma}{1+\Gamma}\right)^2\right)\right]^{1/2} \tag{12}$$

$$\Gamma = \frac{1.18\sqrt{E_{11}E_{33}}}{G_{13}} \tag{13}$$

Where the term $0.42\chi h$ is the correction added to the length of the crack to account for the root rotation of the beam arms [37] and $E_{1f}$is the flexural modulus of the material which was measured for each specimen independently in the current experiments. The above equations do include two rate dependent properties, G_{13} and E_{33} which have been shown to increase by 12% and 25% for strain rates up to 300s^{-1} [38]. Assuming a maximum increase of 25% for these two properties will result in a decrease of 0.11% in the calculated value of G_{IIC}. Therefore, any rate dependency of G_{13} and E_{33} can be ignored.

In the high rate tests it has been argued that the kinetic energy of the body may influence the strain energy release rate at the crack tip [17]. The total kinetic energy of the system is defined as:

$$T = \frac{1}{2}\rho_c B(2h)\int_{-L}^{L}\left(\frac{d\delta}{dt}\right)^2 dx \tag{14}$$

Where ρ_c is the density of the specimen being tested. Therefore the kinetic energy contribution to the strain energy release rate, G (equation (10)) for a specimen with $a/L = 0.5$ was defined to be [17]:

$$\frac{1}{B}\frac{\partial T}{\partial a} = -0.078\rho h\dot{\delta} \tag{15}$$

For the experimental loading rates (maximum $\dot{\delta} \approx 5.5m/s$) investigated, the kinetic energy term can be seen to increase the fracture toughness by less than 1% of G_{IIC}. Therefore it can be reasonably assumed that, for the tests carried out in this investigation, the kinetic energy contribution is negligible and the quasi-static G_{IIC} data reduction procedure to be valid.

2.8 Tensile and Shear strain rate measurement

The displacement, shear and tensile strains were measured using images extracted from video frames in quasi static tests and from high speed photography in the high rate tests. These image sequences were then post processed using a non-contact video extensometer software (Imetrum Ltd) to track specific points on the sample as shown in Figure 7. To verify these measurements, full field strain measurements were carried out using 2D digital image correlation (GOM UK Ltd) for a specimen in each test regime using the same image sequences. A least squares polynomial fit of the first degree (linear fit) was applied to the initial elastic region section of the strain curves to determine the strain rates for all samples respectively.

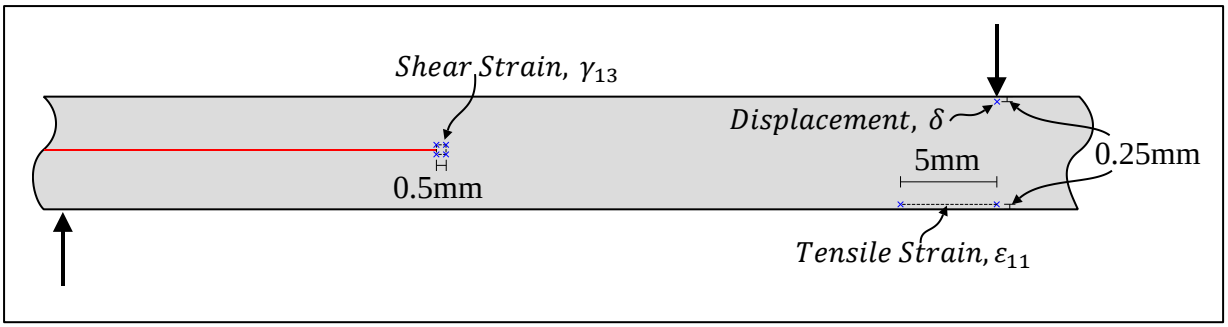

Figure 7 Displacement, tensile and shear strains measured using non-contact video extensometer

3 Results

3.1 Quasi-Static – Data reduction method comparison

The load-displacement plot of the control and pinned samples is shown in Figure 8. The quasi-static flexural tests of all the samples produced an average flexural modulus, E_{1f} of 83.5±1.1GPa. Figure 8 shows the theoretical compliance, calculated using this flexural modulus with $a = 20mm$, $B = 20mm$. The mode II fracture toughness of the initial non pre-crack (from 13µm PTFE release film) was measured to be 1050±156J/m^2. Following the standard ASTM 3ENF test procedure the fracture toughness of the natural pre-crack G_{IIC} of the IM7/8552 was measured to be 663±100J/m^2. Calculating the G_{IIC} using the compliance procedure described in section 2.7 and equation (11) the fracture toughness was measured to be 673±112J/m^2. With only 1.5% difference between the two procedures, the compliance procedure can be accepted to produce correct values of the fracture toughness of the material and gives confidence to use for the high rate procedure.

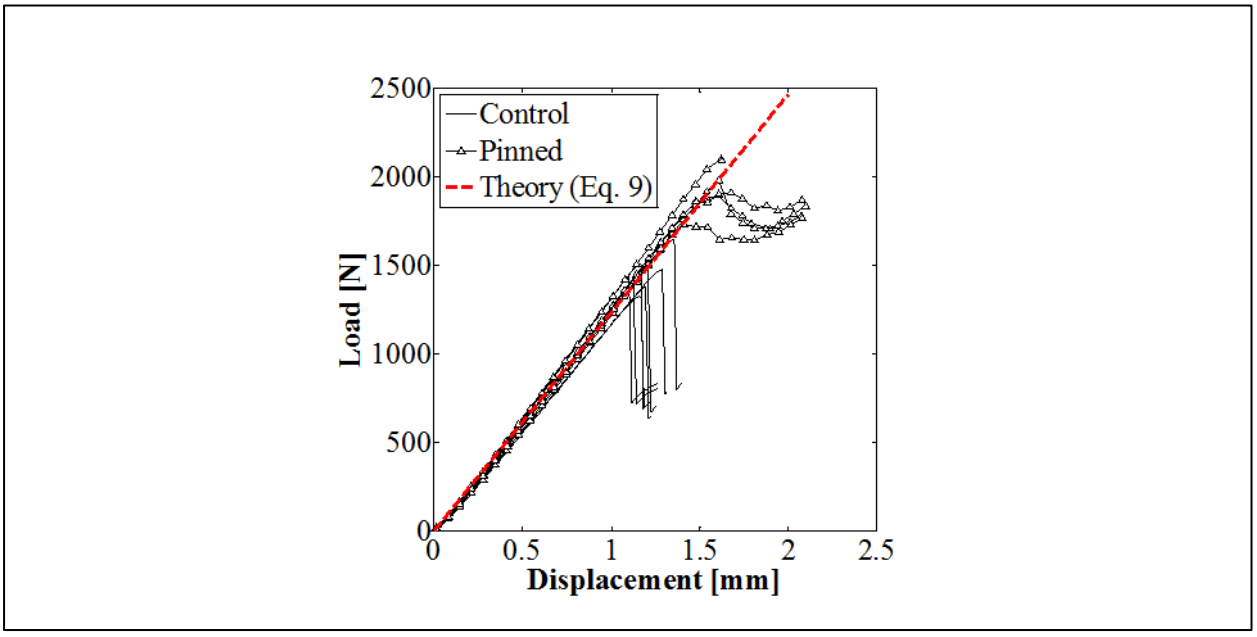

Figure 8 Load-displacement for control specimens along with average compliance using equation (9)

The average R curve for the control and pinned samples are shown in Figure 9. For control samples, the 3ENF only produces a single critical strain energy release rate

value at the moment of initiation due to the unstable nature of the crack, which is the fracture toughness, G_{IIC} of the material. The pinned samples however produce an increasing R curve with crack length due to the development of the extrinsic bridging zone behind the crack tip. The average critical strain energy release rate at the moment of initiation is 922±109J/m^2, a minor increase relative to the control samples. The critical strain energy release rate reaches a maximum of 2613±499J/m^2 at a crack length of 50mm. In this test configuration the maximum bridging zone length possible is 30mm, however the fully developed Z-pin bridging zone length is expected to be much longer than the 30mm length, approximately between 40-60mm [39]. The apparent fracture toughness increase of these tests agrees well with that previously reported in literature [6,39,40].

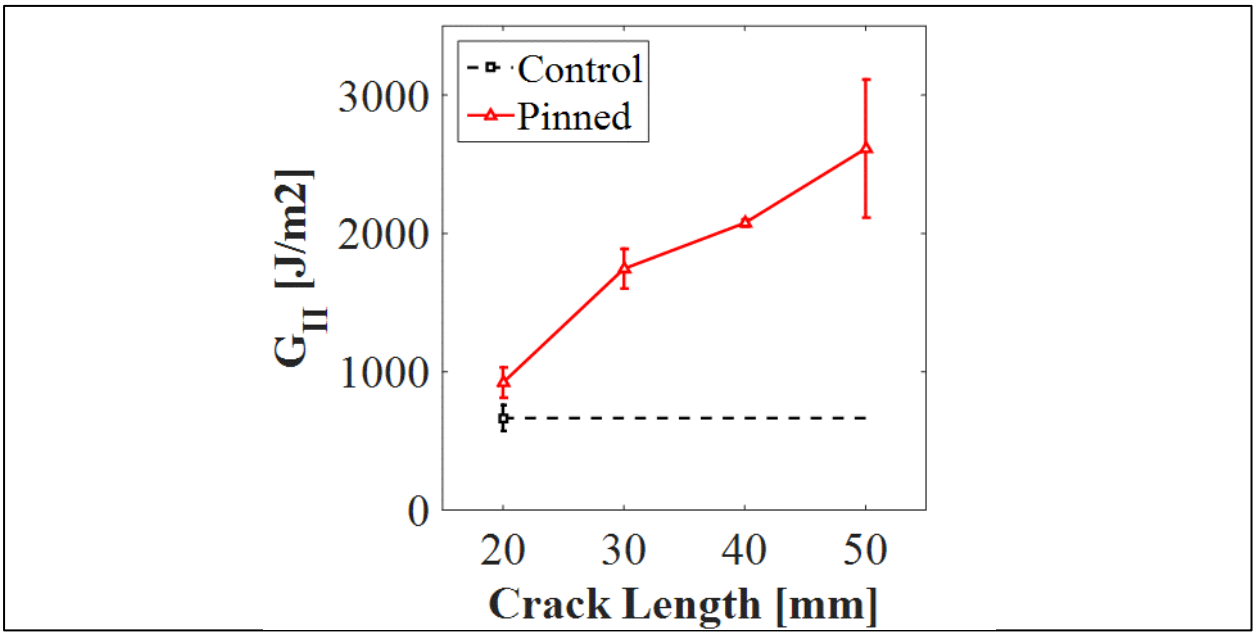

Figure 9 Average R curve for control and pinned specimens

3.2 Delamination velocity

The delamination propagation rate ($\dot{a}$) was measured for each specimen directly from the high speed imaging. An example of the control and pinned response to

delamination initiation is shown in Figure 10. For consistency, $\dot{a}$ was calculated by measuring the time taken for delamination to reach the middle loading nose ~30mm. For control samples the delamination was unstable and typically propagated past the middle loading nose. For the pinned samples the delmination rate varied within this distance, with an almost stick slip behavior.

The relationship between $\dot{a}$ and $\dot{\delta}$ is shown in Figure 11. For the control samples there is a clear almost linear increase in the delamination propagation rate from 444m/s for quasi-static loading rate up to 858m/s for 5.5m/s loading rate. For the pinned samples, the delamination propagation rate was stable ~4mm/s when loaded quasi-statically. The propagation rate increase almost linearly from ~10m/s for 1m/s loading rate up to ~530m/s for 5.5m/s loading rate.

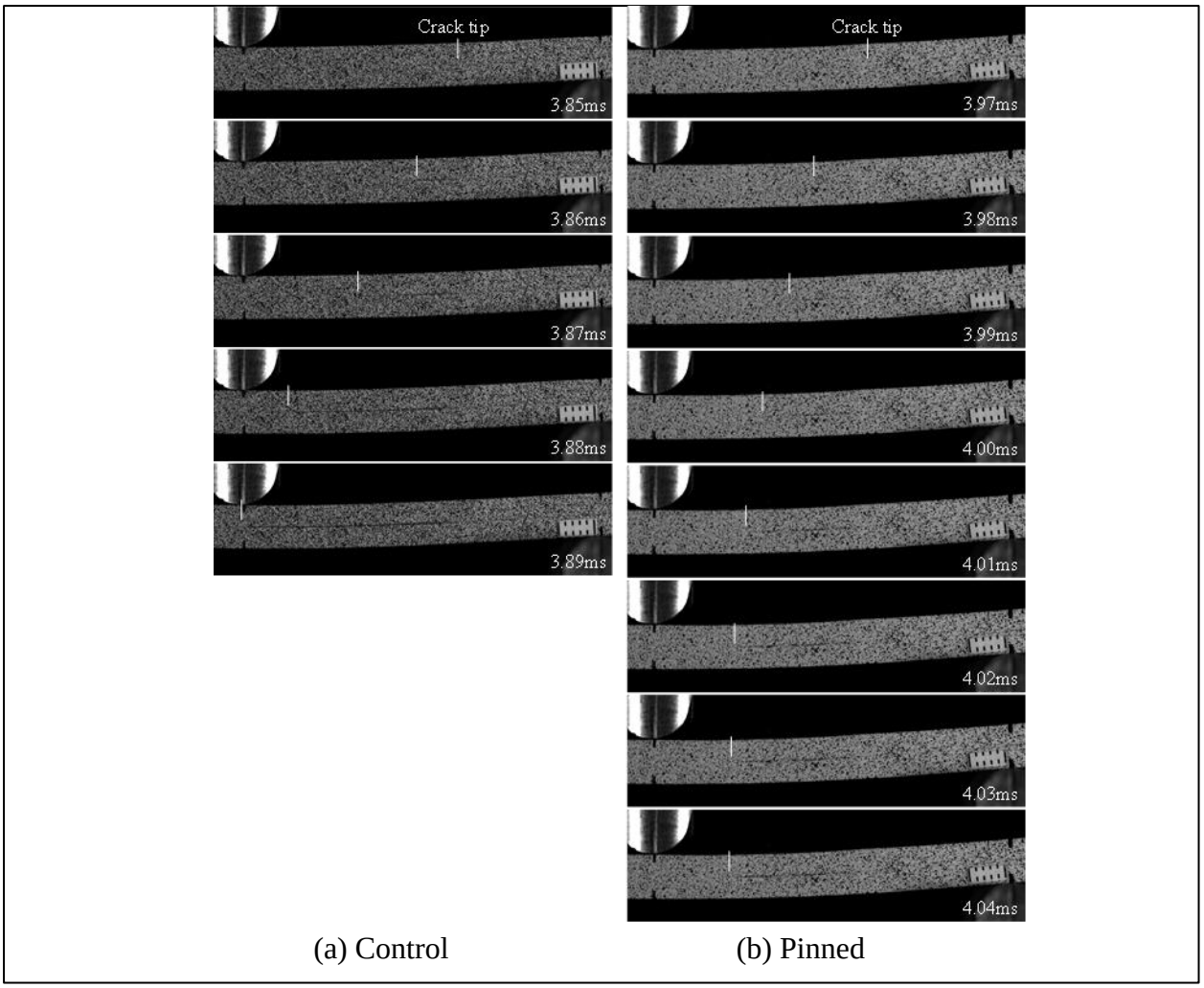

Figure 10 Example of the measurement of average delamination propagation rate ($\dot{a}$) of control and pinned samples tested with loading rate ($\dot{\delta}$) of 3m/s

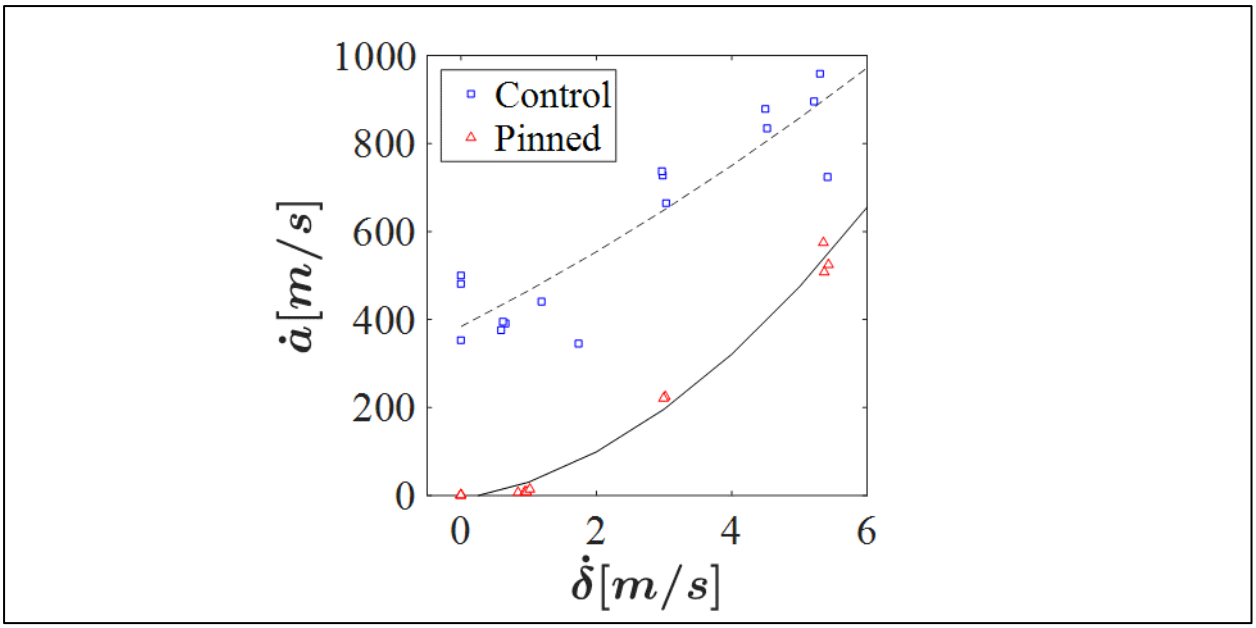

Figure 11 Delamination propagation rate ($\dot{a}$) against loading displacement rate ($\dot{\delta}$)

3.3 Tensile and Shear strain rate response

The relationship of the shear strain rate ($\dot{\gamma}$) measured at the tip of the initial crack and the tensile strain rate ($\dot{\varepsilon}$) measured at the mid span length on the lower surface of the specimen against displacement loading rate ($\dot{\delta}$) is shown in Figure 12. The shear strain rate reaches an average of 22rad/s for samples tested at $\dot{\delta}$ of 5.3m/s. The increase in $\dot{\gamma}$ with $\dot{\delta}$ is approximately linear. The maximum tensile strain rate achieved in this investigation was on average $13s^{-1}$ for samples tested at $\dot{\delta}$ of 5.3m/s.

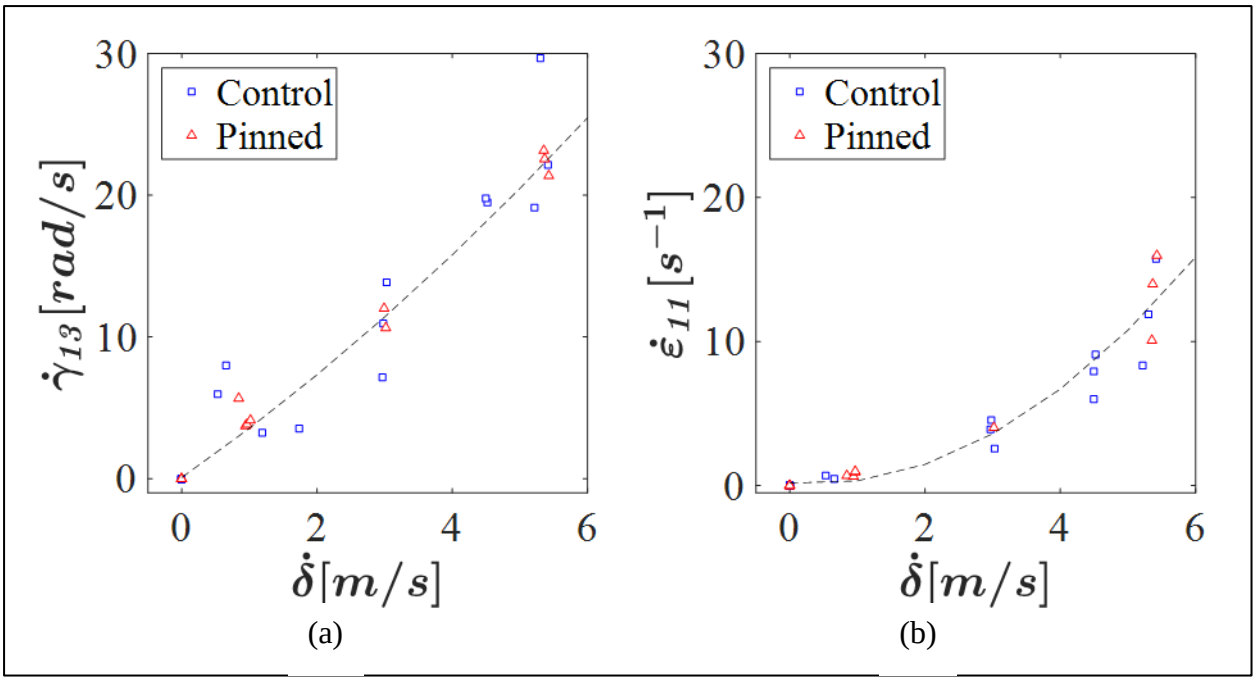

Figure 12 Loading displacement rate ($\dot{\delta}$) against (a) shear strain rate ($\dot{\gamma}$) and (b) tensile strain rate ($\dot{\varepsilon}$)

3.4 Load-displacement response

The load-displacement plots for all the tests are given in Figure 13. With increase in displacement loading rate $\dot{\delta}$ the noise in the load output measured can be seen to increase and produce an unclear critical load prior to delamination. On these plots the loading displacement at which delamination initiated is highlighted. It can be seen that the critical load cannot be taken directly from the load displacement responses necessitating the use of the compliance procedure to calculate the GIIC of the specimens.

For the control samples, the load response appears to be constant with increasing $\dot{\delta}$. For the pinned specimens, there is a significant increase in the initiation load with increase with $\dot{\delta}$. The pinned specimens maintain significant residual interlaminar strength after delamination initiation as compared to the control samples where there is a distinctly sharper load drop.

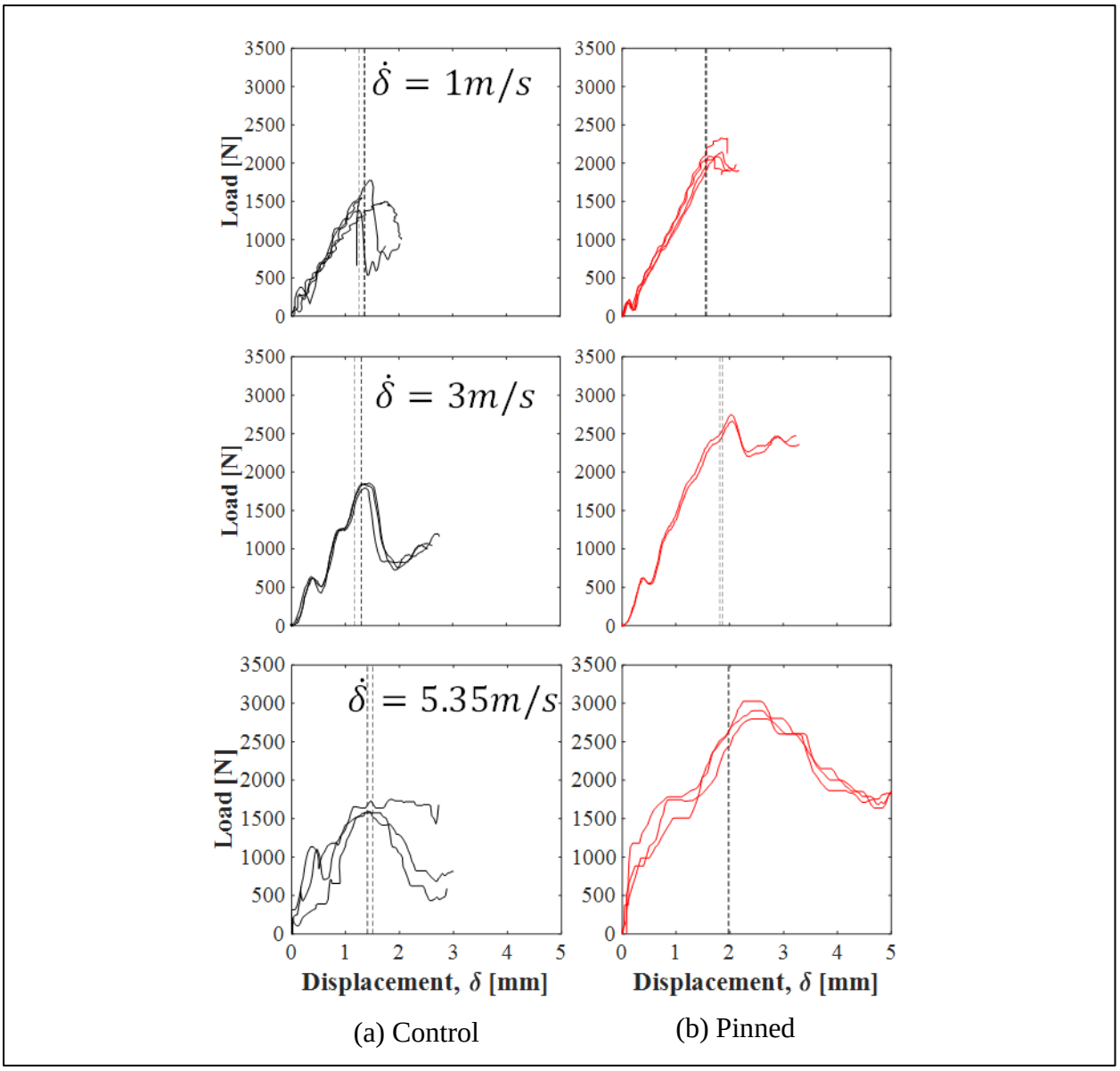

Figure 13 Load-displacement (δ) plots of for increasing loading displacement rate ($\dot{\delta}$), dashed lines indicate the displacement at which delamination initiated

3.5 Rate dependence of interlaminar fracture toughness G_{IIC}

The calculated G_{IIC} at the moment of delamination initiation against loading displacement rate ($\dot{\delta}$), shear strain rate ($\dot{\gamma}$) and delamination velocity ($\dot{a}$) is presented in Figure 14. The control samples produce a minor increase in the G_{IIC} with increase in loading rate from 663±100J/m^2 for quasi-static tests to 970±90J/m^2 for $\dot{\delta}$ of 5.3m/s. The pinned samples showed a very strong increase in G_{IIC} with increase in loading rate. With initiation G_{IIC} of 922±109J/m^2 for quasi-static tests to 2002±64J/m^2 for $\dot{\delta}$ of

5.3m/s. Since the relationship between shear strain rate and displacement rate is almost linear (Figure 12a) the response of G_{IIC} in Figure 14a and Figure 14b produce similar profile. The relationship between GIIC and delamination velocity is approximately linear with very minor increase for the control samples. However, for the pinned samples, there is significant increase in G_{IIC} before what appears to be a plateau forming above 500m/s. Whether the G_{IIC} will increase with increase in delamination velocity will need to be investigated further.

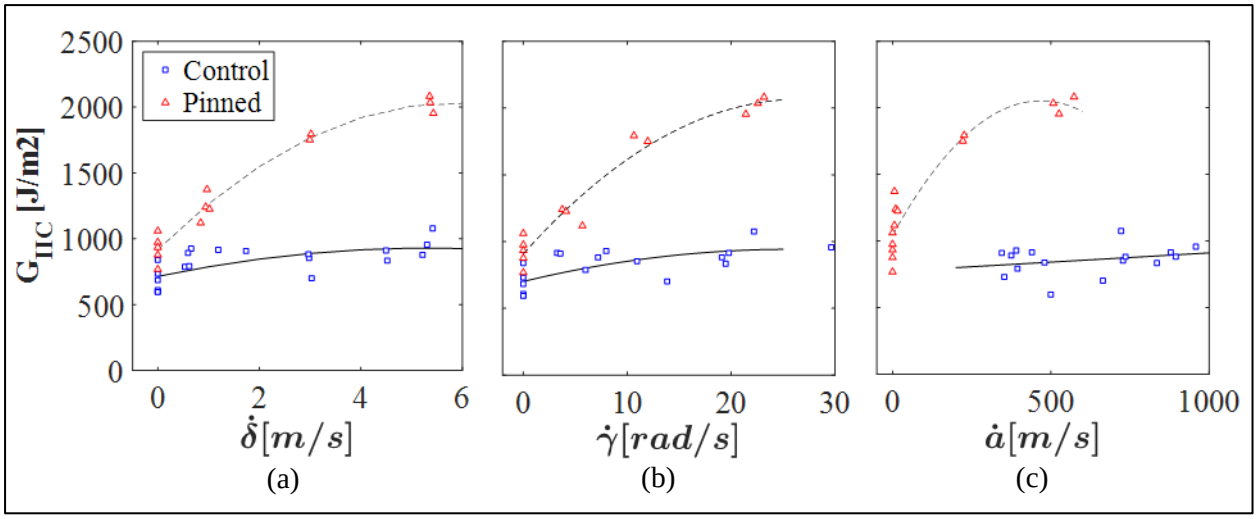

Figure 14 G_{IIC} plots of for increasing (a) loading displacement rate ($\dot{\delta}$), (b) shear strain rate ($\dot{\gamma}$) and (c) delamination velocity ($\dot{a}$)

4 Fractography

A representative control and pinned specimen from each loading rate batch was manually opened and the fracture surface was observed using scanning electron microscope (SEM) imaging. It was seen that the failure profile of the pinned specimens produce two distinct morphology and this morphology was seen to transition for samples tested with loading rates above 3m/s. Figure 15 and Figure 16 show the fracture surfaces of specimens loaded quasi-statically and at a loading rate $\dot{\delta}$ of 5.3m/s respectively. The fracture surfaces of the control samples tested did not

show any significant change in surface profile, with typical shear hackles present. The pinned samples tested quasi-statically showed the standard profile observed in many other mode II fracture tested quasi-statically [6,39,41], in that the pins begin to pull-out, bend and deform before rupture. Figure 15b and c show the small bulge of the pulled-out pin that has been ruptured in a shear dominated form. Pinned specimens exhibiting this failure mode will experience a long mode II bridging zone length and the fracture process observed on a macro scale may be similar to a highly ductile delamination crack.

Figure 16b and c however exhibit a flush, shear failure of the pins. This behavior is reminiscence of a highly brittle fracture and has occurred in specimens tested above 3m/s loading rate. This behavior corresponds to a mode II delamination with a short bridging zone length, since the pins do not have the time to deform, pull-out and rupture. This is highlighted in the increased initiation G_{IIC}. Furthermore, the increase in G_{IIC} does appear to reach an upper level plateau. This limit can be equated to an experimentally and analytically predicted value of approximately 3400J/m^2 for a 0.28mm diameter, T700/BMI pin inserted in an array of 2% nominal areal density [42–44].

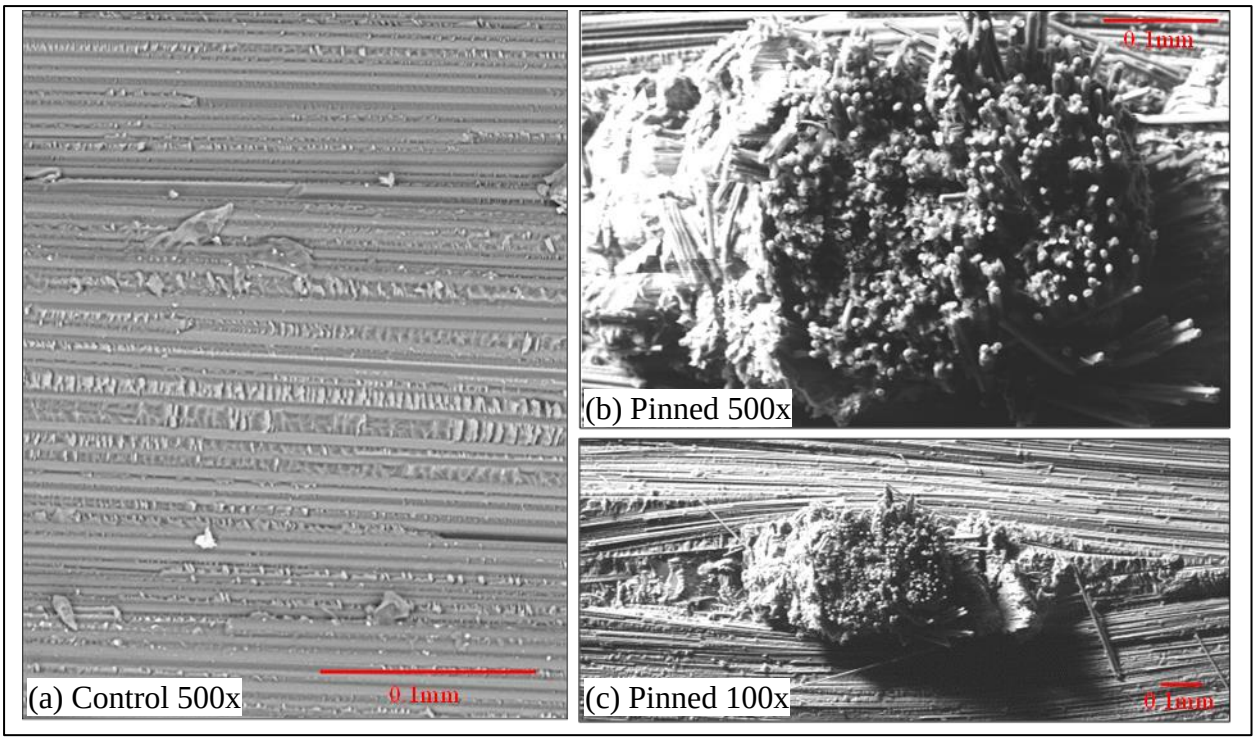

Figure 15 SEM imaging of the fracture surface of (a) control and (b,c) pinned specimens loaded quasi-statically

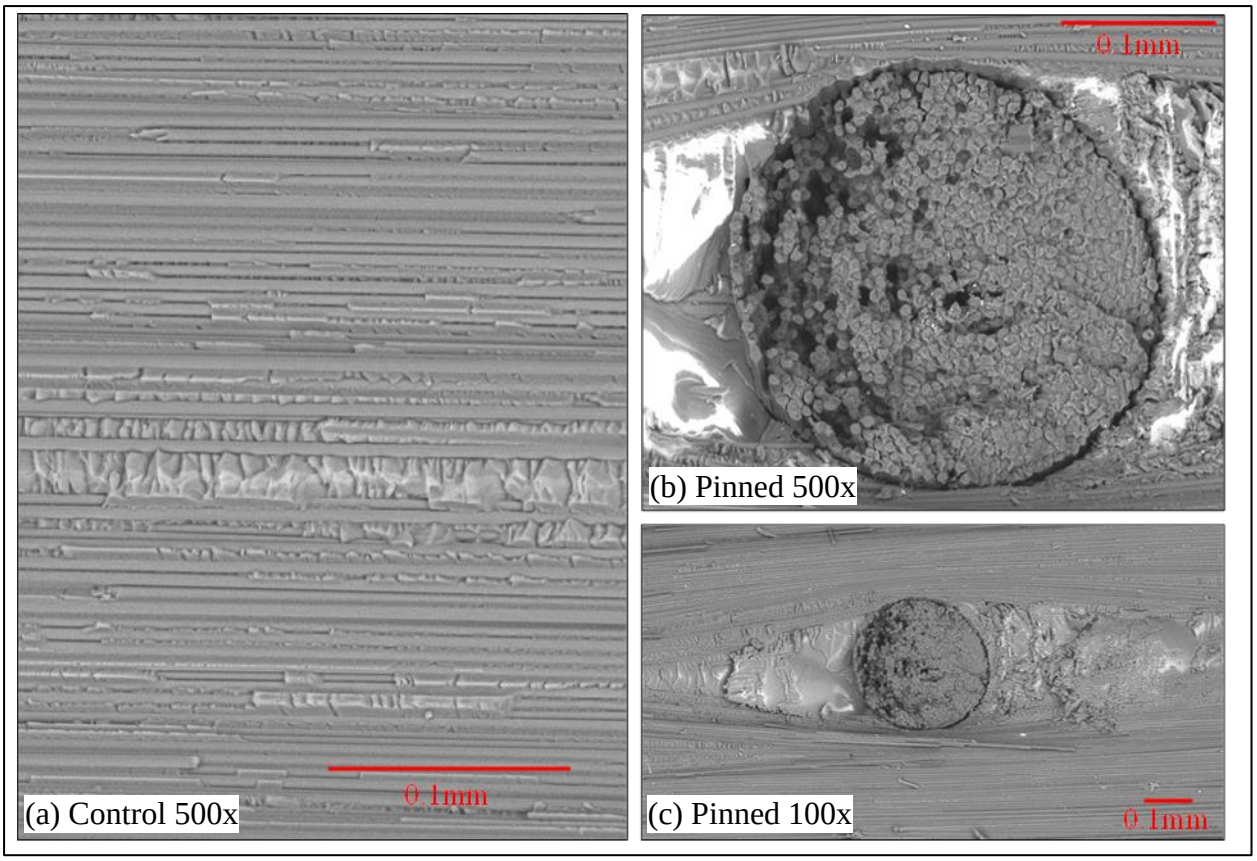

Figure 16 SEM imaging of the fracture surface of (a) control and (b,c) pinned specimens test with loading displacement rate of 5.3m/s

5 Discussions and Conclusions

A comprehensive experimental characterisation of a mode II delamination in a Z-pin reinforced and unreinforced laminated composite has been carried out with increasing strain rates. Tests were performed on standard hydraulic test machines for quasi-static tests, instrumented drop-weight impact tower for intermediate loading rates and a bespoke modified Hopkinson Bar apparatus for high loading rates. The procedure followed to measure the G_{IIC} of the material used a compliance based approach rather that the standard load based data reduction techniques. Assuming that the flexural modulus of the beams are rate independent the G_{IIC} of each specimen was calculated using the loading nose displacement at moment of delamination initiation. This procedure removed the need to deduce the critical load at initiation as the load response was clearly shown to be unreliable due to the excessive dynamic noise in the

436 output results. Furthermore each specimen that was tested was pre-prepared to ensure
437 a natural sharp mode II crack was created and quasi-static test showcased a good
438 agreement in G_{IIC} between the ASTM standard and the compliance method described
439 here.

440 The maximum delamination velocity achieved in the unreinforced tests was on
441 average 858m/s for 5.5m/s displacement loading rate. Falling far below the shear
442 wave speed, calculated for the current IM7/8552 composite system to be 1933m/s.
443 This highlights that higher theoretical delamination propagation rates exist and may
444 be achieved when the composite system is loaded at loading rates above 5m/s. The
445 results show that the average delamination velocity for a composite laminate will
446 increase almost linearly with increasing displacement loading rate. The range of
447 loading rates attempted in this investigation was from quasi-static to ~5.3m/s. The
448 mode II fracture toughness of the composite was seen to have a minor increase from
449 663±100J/m^2 to 970±90J/m^2 confirming behaviours observed in literature for tests on
450 thermosetting brittle epoxy composites, where either minor or no significant increase
451 in G_{IIC} were reported.

452 Mode II delamination in through-thickness reinforced laminates were also
453 characterised. These specimens exhibited a strong apparent fracture toughness
454 increase with displacement loading rate. It was shown that the initiation G_{IIC} increases
455 from 922J/m^2 to 2002J/m^2 over the velocity range tested here. Through fracture
456 surface observations a transition in the failure profile of the Z-pins was revealed. Pins
457 tested at loading rates below 3m/s corresponding to delamination velocity of
458 <<200m/s exhibit a fracture profile similar to those tested quasi-statically, with the
459 pins pulling-out, bending before failing in shear dominated rupture. At higher than
460 3m/s loading rate the delamination velocity in the pinned samples was in excess of

200m/s, this resulted in a very brittle, flat fracture surface of the Z-pins. This highlights that the pins did not have enough time to deform and simply failed in pure shear, with a much larger contribution to the delamination traction forces and a much shorter bridging zone length.

The results highlight how the Z-pinned composites appear to significantly improve the initiation fracture toughness of a composite laminate when loaded at high strain rates ($\dot{\gamma}$>10rad/s). By defining G_{IIZ_min} as the apparent fracture toughness of a crack with a row of Z-pins directly ahead of it (i.e. no extrinsic Z-pins bridging the crack) tested at quasi-static strain rates (if G_{IIZ_min} is not available, this can be set to $G_{IIC}$of the host material), the critical strain energy release rate of a crack behind a row of Z-pins can be defined as the function of shear strain rate $\dot{\gamma}$:

$$G_{IIZ}(\dot{\gamma}) = G_{IIZ_max}\frac{G_{IIZ_min} - G_{IIZ_max}}{1 + \frac{\dot{\gamma}}{m}} \tag{16}$$

Where m is a fitting factor is calculated using a linear least square fit to be 27, Figure 17. The initiation G_{IIC} for the pinned composite does appear to asymptote towards an upper limit, which can be equated to G_{IIZ_max} ≈3400J/m^2, the theoretical maximum apparent toughness for a 0.28mm diameter, T700/BMI pin inserted in an array of 2% nominal areal density, calculated using single pin experiments [42–44].

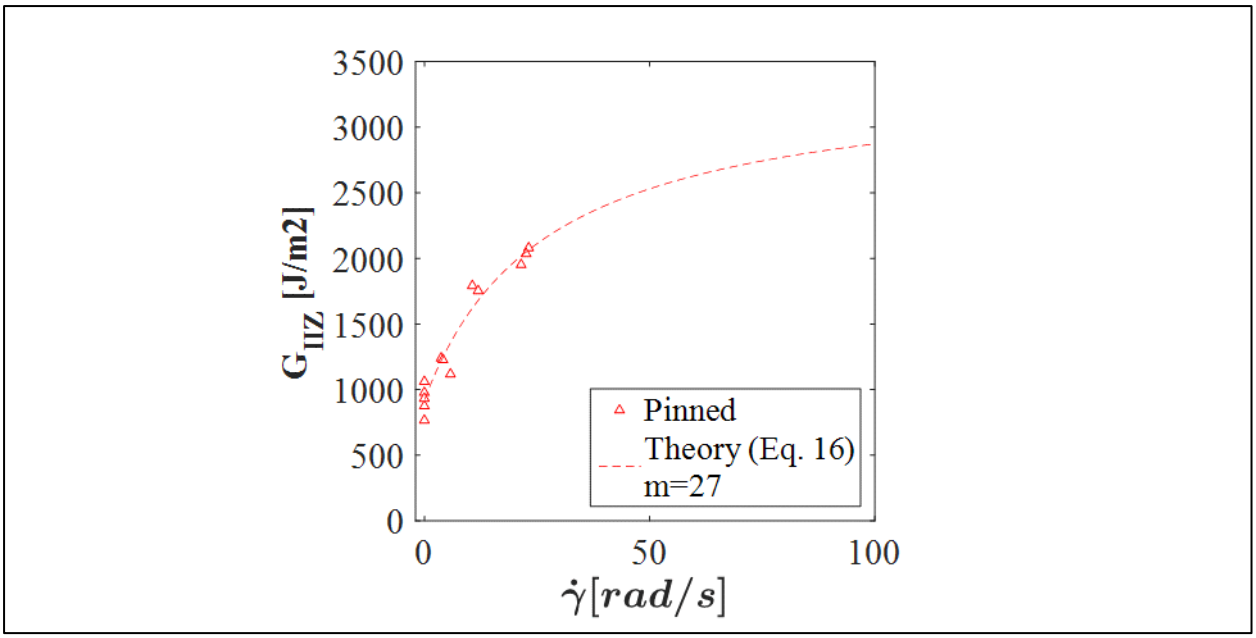

Figure 17 G_{IIZ} plot against shear strain rate ($\dot{\gamma}$) showing the theoretical fit of equation (16) with m=27

The delamination response of unpinned and pinned laminates at higher displacement loading rates is expected to provide the upper plateau for G_{IIC}, G_{IIZ} and the delamination velocity and would be important to characterize experimentally. However, with increasing loading rates, the influence of kinetic energy on the apparent fracture toughness calculations will become more significant and will have to be fully considered. Furthermore, the delamination response to a high energy soft projectile may produce significantly different failure process and thus may be an interesting area to explore.

6 Acknowledgements

The authors would like to acknowledge Rolls-Royce plc for their support of this research through the Composites University Technology Centre (UTC) at the University of Bristol, UK.

7 References

[1] Kinloch AJ, Shaw SJ, Tod DA, Hunston DL. "Deformation and fracture behaviour of a rubber-toughened epoxy: 1. Microstructure and fracture studies," *Polymer*, vol. 24, no. 10, pp. 1341–1354, Oct. 1983.

[2] Shivakumar Gouda PS, Williams JD, Yasaee M, Chatterjee V, Jawali D, Rahatekar SS, Wisnom MR. "Drawdown prepreg coating method using epoxy terminated butadiene nitrile rubber to improve fracture toughness of glass epoxy composites," *Journal of Composite Materials*, May 2015.

[3] Yasaee M, Bond IP, Trask RS, Greenhalgh ES. "Mode I interfacial toughening through discontinuous interleaves for damage suppression and control," *Composites Part A: Applied Science and Manufacturing*, vol. 43, no. 1, pp. 198–207, Jan. 2012.

[4] Yasaee M, Bond IP, Trask RS, Greenhalgh ES. "Mode II interfacial toughening through discontinuous interleaves for damage suppression and control," *Composites Part A: Applied Science and Manufacturing*, vol. 43, no. 1, pp. 121–128, Jan. 2012.

[5] Partridge IK, Yasaee M, Allegri G, Lander JK. "Damage-tolerant composite structures by Z-pinning," in *Toughening Mechanisms in Composite Materials*, Elsevier, 2015, pp. 161–189.

[6] Yasaee M, Mohamed G, Allegri G, Hallett SR. "Mixed mode delamination resistance of Z-pinned multi-directional composites Part I: Experimental Characterisation," *Engineering Fracture Mechanics*, 2016.

[7] Lenzi F, Riccio A, Clarke A, Creemers R. "Coupon tests on z-pinned and unpinned composite samples for damage resistant applications," *Macromolecular Symposia*, vol. 247, pp. 230–237, 2007.

[8] Partridge IK, Cartie DDR. "Delamination resistant laminates by Z-Fiber pinning: Part I manufacture and fracture performance," *Composites Part A: Applied Science and Manufacturing*, vol. 36, no. 1, pp. 55–64, 2005.

[9] Pegorin F, Pingkarawat K, Mouritz AP. "Comparative study of the mode I and mode II delamination fatigue properties of z-pinned aircraft composites," *Materials & Design*, vol. 65, pp. 139–146, Sep. 2014.

[10] Gerlach R, Siviour CR, Wiegand J, Petrinic N. "The Strain Rate Dependent Material Behavior of S-GFRP Extracted from GLARE," *Mechanics of Advanced Materials and Structures*, vol. 20, no. 7, pp. 505–514, Aug. 2013.

[11] Jacob GC, Starbuck JM, Fellers JF, Simunovic S, Boeman RG. "Fracture toughness in random-chopped fiber-reinforced composites and their strain rate dependence," *Journal of Applied Polymer Science*, vol. 100, no. 1, pp. 695–701, 2006.

[12] Kusaka T, Horikawa N, Masuda M. "Low-velocity impact fracture behaviour of impact-resistant polymer matrix composite laminates under mixed mode loading," *Le Journal de Physique IV*, vol. 10, no. PR9, p. Pr9-317-Pr9-322, Sep. 2000.

[13] You H, Yum Y-J. "Loading Rate Effect on Mode I Interlaminar Fracture of Carbon/Epoxy Composite," *Journal of Reinforced Plastics and Composites*, vol. 16, no. 6, pp. 537–549, Apr. 1997.

[14] Kageyama K, Kimpara I. “Delamination failures in polymer composites,” *Materials Science and Engineering A*, vol. 143, no. 1–2, pp. 167–174, 1991.

[15] Blackman BRK, Dear JP, Kinloch a. J, Macgillivray H, Wang Y, Williams JG, Yayla P. “The failure of fibre composites and adhesively bonded fibre composites under high rates of test - Part I Mode I loading-experimental studies,” *Journal of Materials Science*, vol. 30, pp. 5885–5900, 1995.

[16] Compston P, Jar P-YB, Burchill PJ, Takahashi K. “The effect of matrix toughness and loading rate on the mode-II interlaminar fracture toughness of glass-fibre/vinyl-ester composites,” *Composites Science and Technology*, vol. 61, no. 2, pp. 321–333, 2001.

[17] Smiley a. J, Pipes RB. “Rate sensitivity of mode II interlaminar fracture toughness in graphite/epoxy and graphite/PEEK composite materials,” *Composites Science and Technology*, vol. 29, pp. 1–15, 1987.

[18] Mall S, Law GE, Katouzian M. “Loading Rate Effect on Interlaminar Fracture Toughness of A Thermoplastic Composite,” *Journal of Composite Materials*, vol. 21, no. June 1987, pp. 569–579, 1987.

[19] Maikuma H, Gillespie JW, Wilkins DJ. “Mode II Interlaminar Fracture of the Center Notch Flexural Specimen under Impact Loading,” *Journal of Composite Materials*, vol. 24, no. 2, pp. 124–149, Feb. 1990.

[20] Major Z, Lang RW. “Rate Dependent Fracture Toughness of Plastics,” in *European Structural Integrity Society*, vol. 32, 2003, pp. 187–198.

[21] Barton JM. “Epoxy Resins and Composites I,” in *Advances in Polymer Science*, vol. 72, Berlin, Heidelberg, Berlin, Heidelberg: Springer Berlin Heidelberg, 1985, pp. 111–154.

[22] Cox BN, Gao H, Gross D, Rittel D. “Modern topics and challenges in dynamic fracture,” *Journal of the Mechanics and Physics of Solids*, vol. 53, no. 3, pp. 565–596, 2005.

[23] Rosakis AJ. “Intersonic shear cracks and fault ruptures,” *Advances in Physics*, vol. 51, no. 4, pp. 1189–1257, 2002.

[24] Tsai JL, Guo C, Sun CT. “Dynamic delamination fracture toughness in unidirectional polymeric composites,” *Composites Science and Technology*, vol. 61, no. 1, pp. 87–94, 2001.

[25] Colin de Verdiere M, Skordos AA, Walton AC, May M. “Influence of loading rate on the delamination response of untufted and tufted carbon epoxy non-crimp fabric composites/Mode II,” *Engineering Fracture Mechanics*, vol. 96, pp. 1–10, 2012.

[26] Guo C, Sun CT. “Dynamic Mode-I crack-propagation in a carbon/epoxy composite,” *Composites Science and Technology*, vol. 58, no. 9, pp. 1405–1410, 1998.

[27] Jiang W, Tjong S, Chu P, Li R. “Interlaminar Fracture Properties of Carbon Fibre/Epoxy Matrix Composites Interleaved with Polyethylene Terephthalate (PET) Films,” *Polymers and Polymer Composites*, vol. 9, no. 2, pp. 141–146, 2001.

[28] Liu H, Yan W, Yu X, Mai Y. “Experimental study on effect of loading rate on mode I delamination of z-pin reinforced laminates,” *Composites Science and*

Technology, vol. 67, no. 7–8, pp. 1294–1301, Jun. 2007.

[29] Andrew Schlueter, Parab ND, Chen W. "Loading rate effects on mode I delamination of Z-pinned composite laminates," in *Dynamic Behavior of Materials, Volume 1*, Cham, B. Song, D. Casem, and J. Kimberley, Eds. Cham: Springer International Publishing, 2014.

[30] ASTM-D7905-14. "Standard Test Method for Determination of the Mode II Interlaminar Fracture Toughness of Unidirectional Fiber-Reinforced Polymer Matrix Composites," *ASTM International*, 2014.

[31] ASTM D790-07. "Standard test methods for flexural properties of unreinforced and reinforced plastics and electrical insulating materials," *ASTM International*, vol. (2007)e1, 2007.

[32] Hallett SR. "Three-point beam impact tests on T300/914 carbon-fibre composites," *Composites Science and Technology*, vol. 60, no. 1, pp. 115–124, Jan. 2000.

[33] Gerlach R, Siviour CR, Petrinic N, Wiegand J. "Experimental characterisation and constitutive modelling of RTM-6 resin under impact loading," *Polymer*, vol. 49, no. 11, pp. 2728–2737, 2008.

[34] Wiegand J, Hornig a., Gerlach R, Neale C, Petrinic N, Hufenbach W. "An Experimental Method for Dynamic Delamination Analysis of Composite Materials by Impact Bending," *Mechanics of Advanced Materials and Structures*, vol. 22, no. 5, pp. 413–421, 2015.

[35] Weeks CA, Sun CT. "Modeling non-linear rate-dependent behavior in fiber-reinforced composites," *Composites Science and Technology*, vol. 58, no. 3–4, pp. 603–611, Mar. 1998.

[36] de Moura MFSF, de Morais AB. "Equivalent crack based analyses of ENF and ELS tests," *Engineering Fracture Mechanics*, vol. 75, pp. 2584–2596, 2008.

[37] Wang Y, Williams JG. "Corrections for mode II fracture toughness specimens of composites materials," *Composites Science and Technology*, vol. 43, no. 3, pp. 251–256, 1992.

[38] Koerber H, Xavier J, Camanho PP. "High strain rate characterisation of unidirectional carbon-epoxy IM7-8552 in transverse compression and in-plane shear using digital image correlation," *Mechanics of Materials*, vol. 42, no. 11, pp. 1004–1019, 2010.

[39] Pegorin F, Pingkarawat K, Daynes S, Mouritz AP. "Mode II interlaminar fatigue properties of z-pinned carbon fibre reinforced epoxy composites," *Composites Part A: Applied Science and Manufacturing*, Aug. 2014.

[40] Cartie DDR, Troulis M, Partridge IK. "Delamination of Z-pinned carbon fibre reinforced laminates," *Composites Science and Technology*, vol. 66, pp. 855–861, 2006.

[41] Yasaee M, Mohamed G, Hallett SR. "Multiple delamination interaction in Z-pinned composites in Mode II," *Experimental Mechanics*, 2016.

[42] Yasaee M, Lander J, Allegri G, Hallett S. "Experimental characterisation of mixed mode traction–displacement relationships for a single carbon composite Z-pin," *Composites Science and Technology*, vol. 94, pp. 123–131, 2014.

[43] Allegri G, Yasaee M, Partridge IK, Hallett SR. "A novel model of

delamination bridging via Z-pins in composite laminates," *International Journal of Solids and Structures*, vol. 51, no. 19–20, pp. 3314–3332, Oct. 2014.

[44] Zhang B, Yasaee M, Hallett SR, Allegri G. "Micro-Mechanical Finite Element Analysis of Z-pins under Mixed-Mode Loading," *Composites Part A: Applied Science and Manufacturing*, 2015.

https://dspace.org/

Strain rate dependence of mode II delamination resistance in through thickness reinforced laminated composites

Yasaee, Mehdi; Mohamed, Galal; Pellegrino, Antonio; Petrinic, Nik; Hallett, Stephen R.

2017-05-04
Elsevier
http://dx.doi.org/10.1016/j.ijimpeng.2017.05.003
Yasaee M, Mohamed G, Pellegrino A, Petrinic N, Hallett SR, Strain rate dependence of mode II delamination resistance in through thickness reinforced laminated composites, International Journal of Impact Engineering, Volume 107, September 2017, Pages 1–11.

Downloaded from a DSpace repository. https://dspace.org/